Geotech Geol Eng
https://doi.org/10.1007/s10706-018-0539-2

ORIGINAL PAPER

Deep Cement Mixed Walls with Steel Inclusions for Excavation Support

R. Nishanthan · D. S. Liyanapathirana · C. J. Leo

Received: 17 August 2015 / Accepted: 30 March 2018

Abstract Deep cement mixed (DCM) walls are widely used in supporting excavations in many parts of the world. In this paper, a case study of an excavation supported by a DCM wall with steel inclusions is analysed using a three-dimensional finite element model and based on the coupled theory of nonlinear porous media. The DCM wall is constructed with wide flange steel inclusions. The stress–strain behaviour of the DCM wall section is simulated using an extended version of the Mohr–Coulomb model, which considers the strain-softening behaviour of DCM columns beyond yield. The computed lateral deformations are compared with the field measurements to validate the numerical modelling procedure. Using the same case study, the internal stability of the wall against bending and shear failure modes is investigated. In addition, the lateral pressure distribution along the wall length is investigated because in practice design is carried out considering a uniform pressure distribution assuming rigid wall movements. A parametric study was carried out to investigate the viability of DCM walls in supporting excavations by varying the spacing between steel inclusions, wall thickness and initial lateral earth pressure. Based on the results of the parametric study, guidelines are proposed to select the most efficient geometric arrangement of steel inclusions within DCM walls.

Keywords Excavation support · Deep cement mixed columns · Steel inclusions · Finite element method · Strain softening · Ground movements

1 Introduction

Deep cement mixed (DCM) retaining walls are used in practice to support excavations due to a number of advantages offered by them. They have the ability to: reduce the ground movements due to excavations, increase the bearing capacity, prevent sliding failure, minimise base heave and control seepage by acting as cut-off barriers (Rutherford et al. 2005). In general, these walls are self-supporting gravity structures or structures supported by external elements such as anchors or bracings. Due to very low tensile strength of cement stabilised soils, DCM walls do not have enough lateral load carrying capacity. Hence in practice, steel inclusions are used in DCM walls to increase the tensile strength. In addition, different column configurations have been used to utilise the compressive strength of DCM walls efficiently, while reducing the development of tensile stresses.

R. Nishanthan · D. S. Liyanapathirana (✉) · C. J. Leo
School of Computing, Engineering and Mathematics, University of Western Sydney, Locked Bag 1797, Penrith, NSW 2751, Australia
e-mail: s.liyanapathirana@uws.edu.au

Published online: 19 April 2018

The early applications of DCM walls consist of gravity retaining structures with large cross sections to resist lateral loads applied on them without any steel inclusions. The gravity structures with rows of continuous parallel DCM walls in a discontinuous web structure proposed by Shao et al. (1998) and Vertical Earth Reinforcement Technology (VERT) walls introduced by Nicholson et al. (1998) are examples of gravity walls without steel inclusions. In VERT wall systems, a row of secant DCM columns is formed at the excavation front. Then, rows of isolated DCM columns are formed behind the secant columns to provide additional vertical reinforcement within the retained soil. The clear spacing between DCM columns and the number of isolated column rows depend on the excavation problem considered. Finally, DCM columns are capped together using soil slurry spoils ejected from each hole to ensure that the DCM columns and soil act as a composite gravity wall and to provide a relieving platform for surcharge loads. Nicholson et al. (1998) evaluated the effect of spacing, soil cement strength and layout patterns by carrying out finite element modelling considering the configuration of these composite walls. Briaud et al. (2000) proposed to reinforce the front columns of VERT wall systems to ensure the factor of safety against cracking due to tensile stresses developed due to bending. Based on the full-scale VERT walls constructed in a sandy soil at the National Geotechnical Experimentation site at Texas A&M University, they discussed five modes of deformation: pure shear deformation, rigid body rotation, rigid body translation, rigid body settlement and bending.

Another type of DCM walls used successfully in practice without any reinforcement is the arch-shaped retaining walls. This is possible because arches support loads by resolving them into compressive stresses, eliminating development of tensile stresses. In a case study reported by Blackwell (1992), a circular DCM column structure consisting of three concentric unreinforced overlapping rings of 750-mm-diameter columns is constructed to support manholes. Shao et al. (2005) reported a case study of an arch-shaped earth retaining structure to support a 9-m-deep excavation, where the wall is constructed using a series of arches. Each arch is restrained at the ends using reinforced concrete bored piles. Use of semicircular (polygon) structures for DCM retaining walls was reported by Stoetzer et al. (2006) and Capelo et al. (2012).

When constructing arch-shaped walls, circular attached DCM columns are formed using the conventional method, where columns are formed by augers rotating about the vertical axis. However, construction of planar walls is more convenient in practice compared to construction of arch-shaped walls, although planar walls need steel inclusions to carry tensile stresses. In 2003, Bauer Maschinen Group in Germany developed the Cutter Soil Mixing (CSM) technology to improve the efficiency of construction of planar walls, where rectangular overlapping DCM panels are formed using vertical counter rotating wheels about the horizontal axis (Gerressen and Vohs 2012). In both construction methods (attached DCM columns and CSM technology), wide flange beams are inserted in the planar walls before the hardening of the slurry to enhance the lateral load carrying capacity of the retaining structure. In recent years, DCM walls with steel inclusions are widely used in practice for excavation support and as seepage barriers in many projects (Yang 2003; Rutherford et al. 2007; Lopez et al. 2009; Parmantier et al. 2009; Gerressen and Vohs 2012).

This paper presents a three-dimensional numerical modelling of a well-documented case study. In this case, a planar DCM wall with steel inclusions was used to support an excavation, which was carried out for the Islais Creek Transport/Storage project in San Francisco. An extended version of the elasto-plastic Mohr–Coulomb constitutive model is used to incorporate the strain-softening behaviour of cement stabilised soils. ABAQUS/Standard finite element programme is used for finite element modelling, and the extended version of the Mohr–Coulomb model, which has the ability to simulate the strain-softening behaviour of cement stabilised soils, is incorporated into the ABAQUS/Standard as a user-defined subroutine. Using the same problem, the stability of the DCM wall was investigated for bending and shear failure modes. In practice, lateral pressure acting along the wall length is assumed to be uniform considering rigid wall movements. However, for wall systems with soldier piles and timber lagging, due to the substantial stiffness difference between piles and timber lagging, timber lagging tends to deform higher than piles. This leads to formation of arches between stiffer piles developing a pressure variation along the wall length

(MacNab 2002; Perko and Boulden 2008; Vermeer et al. 2001). Since DCM walls with steel inclusions are similar to soldier piles with timber lagging, the significance of pressure variation along the wall on the overall behaviour of the DCM wall with steel inclusions is investigated. Finally, a parametric study is carried out to investigate the influence of distance between steel inclusions, lateral pressure acting over the wall and thickness of the DCM wall, on the stress variation inside the cement stabilised wall section. Based on these results, guidelines are proposed for the selection of the most efficient geometric arrangement for DCM walls with steel inclusions.

2 Constitutive Model for DCM Columns

Majority of finite element studies found in the literature, simple constitutive models were used to simulate the behaviour of DCM columns. Mohr–Coulomb model was used by Shao et al. (1998), Huang et al. (2009) and Lai et al. (2006), and the hyperbolic model was used by Nicholson et al. (1998) and Ou et al. (1996). These models do not have the ability to simulate the breakage of soil–cement structure and subsequent strain-softening behaviour of the cement stabilised soils. There are constitutive models within the critical state framework to represent the behaviour of cement stabilised soils incorporating the breakage of soil cement structure during loading (e.g. Vatsala et al. 2001; Lee et al. 2004; Suebsuk et al. 2010; Arroyo et al. 2012; Nguyen et al. 2014). The constitutive models developed by Nguyen et al. (2014) and Nguyen and Fatahi (2016) show very good agreement with triaxial test data of cement mixed soils under both high and low confining pressures, and well captures the degradation of cementation bonds during loading under triaxial loading conditions. However, the non-associated plasticity used in their model formulation makes it difficult to apply in solving boundary value problems due to extremely large matrix storage requirements. In the literature, no studies can be found employing these constitutive models within the critical state framework to solve boundary value problems due to complexity in implementing them in commercially available finite element programmes and associated numerical instability problems.

Constitutive models based on the Mohr–Coulomb criteria with strain-softening behaviour were implemented successfully to analyse the failure modes in embankment construction and cut slopes in clayey soils using the finite element method (e.g. Potts et al. 1990, 1997). These models have the ability to simulate the peak and residual behaviour shown by cement stabilised soils as well as the increase in strength and stiffness due to cementation. According to Quiroga et al. (2017), the strength increase is about 8–19 times and the stiffness increase is about 4–6 times, when the cement content increased from 10 to 20%.

In these models, strain-softening, which characterise the peak and residual behaviour, was modelled as a reduction in friction angle and cohesion with increasing plastic deviatoric strain of the cement stabilised soil. In the current analysis, an approach similar to Yapage et al. (2015), which is an extended version of the Mohr–Coulomb failure criteria, is used to simulate the isotropic strain-softening behaviour of cement stabilised soils. As shown in Fig. 1, strength parameters are constant at the peak values of cohesion (c_p), friction angle (φ_p) and dilation angle (ψ_p), until the plastic deviatoric strain reaches the peak, $\gamma^p_{d,\text{peak}}$. Then, the strength parameters start to decrease until the stress state reaches its residual state (φ_{res}, c_{res}, ψ_{res}) until the plastic deviatoric strain reaches the residual, $\gamma^p_{d,\text{res}}$, and beyond that strength parameters stay constant at the residual values. This model is implemented in ABAQUS/Standard finite element programme used in this study, using the user-defined subroutine, USDFLD.

3 Case Study

For the Islais Creek Transport/Storage Project in San Francisco, California, a 12-m-deep excavation was carried out for the construction of a sewer box and an overflow structure (Rutherford et al. 2007). Excavation was supported by a DCM wall, where wide flange H-beams were inserted in alternative columns of the wall to function as soldier piles. The wide flange columns (W30 × 108) used have a bending stiffness of 304.6 MNm^2/m. The DCM wall is internally braced by three levels of struts as shown in Fig. 2, and it was constructed using 910-mm-diameter attached DCM columns at 1.3 m centre to centre spacing. The

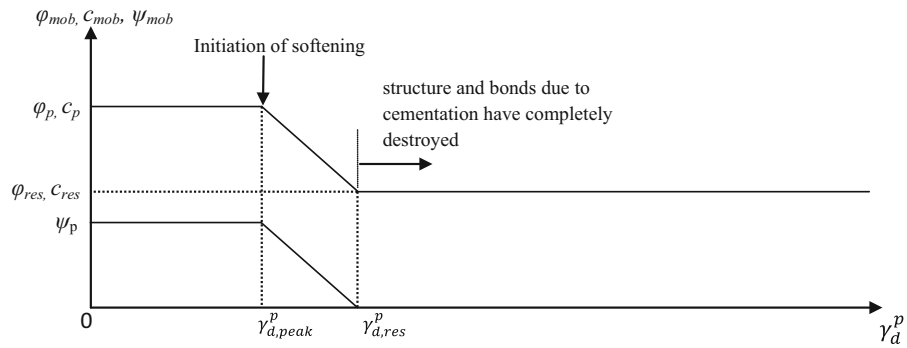

Fig. 1 Variation of mobilised friction angle φ_{mob}, cohesion, c_{mob} and dilation angle ψ_{mob} with plastic deviatoric strain, γ^p_d

excavation is 11.7 m deep and 11.0 m wide. The subsurface soil layout and properties of each layer at the site are given in Table 1. The upper most 5.5-m-thick layer is a fill. The fill layer is underlain by an 8.5-m-thick layer of bay mud, which is a soft to medium stiff layer of plastic clay, dark grey in colour. Below the bay mud layer there is a 1.8-m-thick layer of Marine sand. Above the bedrock of the Franciscan formation and below the Marine sand layer, there is a colluvium deposit starting from 15.8 m below the surface, as shown in Fig. 2. The water table is found at a depth of 8.4 m below the ground surface.

3.1 Material Properties for Soil and DCM Wall

An effective stress-based finite element analysis was carried out using the finite element method. The stress–strain behaviour of the soil layers was simulated using the Mohr–Coulomb criteria with non-associated flow rule. Properties for soil layers shown in Fig. 2 were extracted from Rutherford et al. (2007). DCM columns were modelled using the extended version of Mohr–Coulomb model explained in Sect. 2. For the DCM columns used in this study, field or laboratory data are not available to extract the material properties. Hence in this study, peak friction angle (φ'_p) is assumed as 30° (EuroSoilStab 2002; Yapage et al. 2015). According to Yapage et al. (2015), peak cohesion of cement stabilised soil (c'_p) is assumed to be 0.289 times the unconfined compressive strength (q_u). For the current analysis, a value of 578 kPa was assumed for c'_p based on the data given by Yapage et al. (2015) for cement stabilised soils. Softening index, which is the ratio between residual strength parameters and peak strength parameters, ranges from 0.4–0.7 to 0.4–0.8 for cohesion and friction angle, respectively (Yapage et al. 2015). In this study, the same softening index of 0.4 is assumed for both cohesion and friction angle ($\varphi'_{p,\text{res}} = 12°$ and $c'_{p,\text{res}} = 230$ kPa). Plastic deviatoric strain terms at peak ($\gamma^p_{d,\text{peak}}$) and residual ($\gamma^p_{d,\text{res}}$) values are assumed to be 2 and 12%, respectively, based on the results given by Yapage et al. (2015). For the elastic modulus of DCM columns, McGinn and O'Rourke (2003) proposed a value of $150q_u$ for columns constructed using the wet mixing method. Porbaha et al. (2000) and Ellen et al. (2013) proposed a value of $100q_u$ and $300q_u$, respectively. For the finite element analysis presented in this paper, a value equivalent $100q_u$ is assumed for the elastic modulus of DCM walls, which is equal to 200 MPa. Permeability of treated soil is generally lower than the unstabilised soil (Okumura 1996; Broms 1999). Ellen et al. (2013) and Taki and Yang (1991) recommended permeability between 10^{-5} and 10^{-6} cm/s for excavation support and ground water control. In this case a value of 1×10^{-4} m/day, which is lower than that of the parent soil, is assigned for the DCM wall.

3.2 Finite Element Analysis

The case study was modelled using a three-dimensional finite element model, and the results were compared with the measured field data. Soil and DCM wall below the water table are modelled using twenty-node brick elements with pore pressure degrees of freedom at the corner nodes and the reduced integration. All other parts of the finite element mesh above the water table are developed using twenty-node brick elements with reduced integration but without any

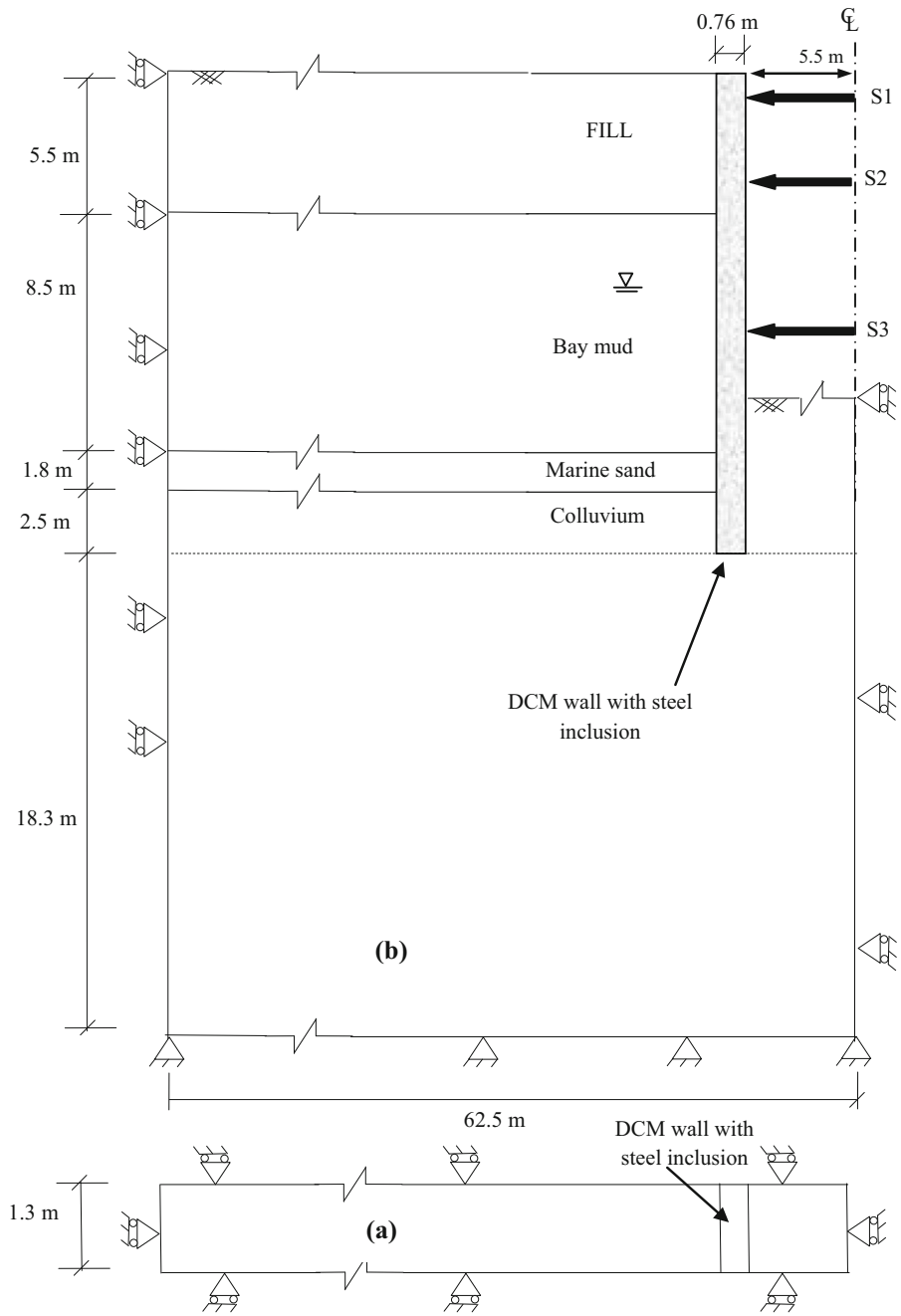

Fig. 2 Cross section and plan view of the excavation

pore pressure degrees of freedom. Only half of the repetitive section of the problem was modelled due to the symmetry of the loading and geometry of the problem. The finite element mesh used for the analysis is extended four times the depth of the excavation from the centre of the excavation, and the bottom mesh boundary is located 24.9 m below the bottom of the excavation, which is more than twice the depth of the excavation, as shown in Fig. 2. Boundary conditions used in the finite element model are as follows: (1) bottom of the mesh is restricted against both horizontal and vertical movements and (2) four vertical faces of

Table 1 Material properties used in the numerical modelling

Material	E (MPa)	v	c' (kPa)	φ' (°)	γ (kN/m^3)	k (m/day)
Fill	8	0.3	0.2	35	19.2	1.0
Bay mud	10	0.35	35	0.1	14.6	0.001
Marine sand	12	0.35	0.2	37	20.6	1.0
Colluvium	12	0.3	0.2	40	20.4	1.0
DCM columns	200	0.3	578 (peak)	30 (peak)	20.0	1×10^{-4}

E is elastic modulus, v is Poisson's ratio, γ is the unit weight (saturated and unsaturated unit weight for soils below and above the ground water table respectively), c' is the effective cohesion intercept, φ' is the effective friction angle, and k is the coefficient of permeability

the three-dimensional finite element mesh are allowed to move along the plane of each face, but the movements are restricted in the directions perpendicular to each vertical face of the mesh.

A no slip condition was assumed along the DCM wall–soil interface. Due to the wet mixing method used at the site for the construction of the DCM wall, this is a reasonable assumption. At the steel–DCM wall interface, severe convergence problems were encountered when a contact algorithm with a penalty contact allowing separation at the interface was introduced due to the geometry of the H-beam section with corners as illustrated in Fig. 3. Hence, a no slip condition was assumed at the steel–DCM wall interface as well.

When using ABAQUS for soil modelling based on the coupled theory of nonlinear porous media, there are two approaches available in terms of effective stresses. It is very important to understand them because only one approach is applicable for modelling excavations. In the first approach, initial geostatic stress state is established applying the soil weight as a body load. Then, the pore pressures used in the analysis are excess pore pressures without incorporating the hydrostatic water pressures. In this approach, when finite elements are removed to simulate the excavation and water table is lowered within the excavation, unbalanced hydrostatic forces acting on the wall due to the water table within the retained soil are not applied on the wall. Hence, wall deformations are under predicted by the finite element analysis. In the second approach, initial geostatic stress state is established applying the soil weight as a gravity load. Then, the analysis is carried out considering total pore pressures. In this approach, when the elements are removed to simulate the excavation, it will lower the water table within the excavation up to the excavated surface. Since total pore pressures are considered in the analysis, the appropriate unbalanced hydrostatic pressure is automatically established behind the wall considering the water table within the retained soil. Hence, the results presented in this paper are based on the second approach with gravity loading.

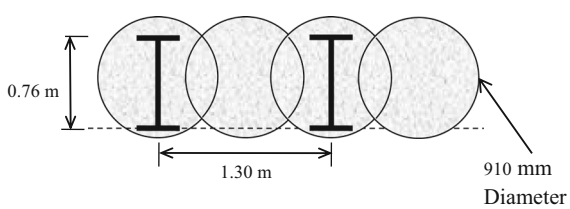

Fig. 3 Typical section of DCM and wide flange columns

The analysis neglected the installation effects for the wide flange H-beams and DCM walls. It is assumed that there is no change in the initial geostatic stress state during the construction of DCM wall. The reason for this assumption is that it is impossible to numerically simulate the mechanics of cement–soil mixing process and the deep penetration of the steel beams with the existing capabilities of the finite element programme used for this study, ABAQUS. Hence, the wall behaviour presented in this paper is induced entirely due to the excavation and installation of struts. Construction sequence was simulated in eight stages. In the first stage, geostatic equilibrium is achieved using the initial stresses due to material weight and the coefficient of earth pressure at rest. In the step by step excavation process, removal of soil and installation of struts were simulated by removal of finite elements representing soil and addition of spring elements, respectively. Throughout the excavation,

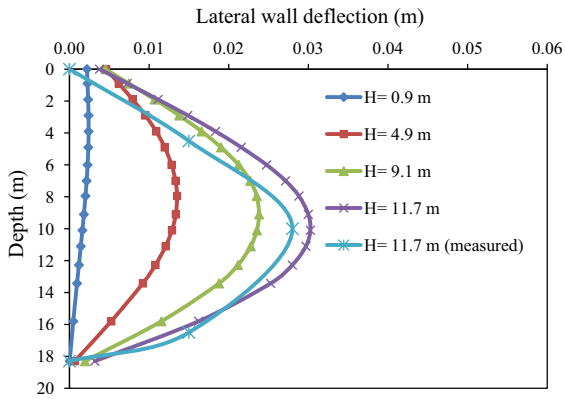

Fig. 4 Lateral wall movement at different stages of the excavation

water level inside the excavation was maintained 1 m below the newly excavated surface to avoid unrealistic heave and associated convergence problems.

Figure 4 shows the progressive movement of wall at different stages of the excavation. At all excavation depths, beyond the 0.9-m excavation, maximum wall deformation occurred around mid-depth of the wall. Only the wall movement measured at the end of 11.7 m of excavation, which is the final excavation stage, is available from the case study. According to Fig. 4, the computed wall movement at the final stage of the excavation agrees well with the measured wall movement. Therefore, it can be concluded that the numerical procedure adopted in this case with no slip condition at the DCM–soil and steel–DCM interfaces, and the establishment of the geostatic equilibrium using the gravity load option is appropriate to predict the wall deformations during excavations adequately. A shift was predicted near the wall base during the initial stages of the excavation, but the magnitude of the shift is negligible compared to the overall wall deformation. In this case, there is no sign of yielding of DCM columns observed during the excavation.

3.3 Internal Stability of the Wall

According to Briaud et al. (2000), there are five modes of deformation needs to be considered when investigating the stability of DCM walls: pure shear deformation, rigid body rotation, rigid body translation, rigid body settlement and bending. In this section, the stability of the wall described in the previous section was investigated considering shear and bending failure modes because the rigid body deformations such as rotation, translation and settlement were insignificant for this case based on the numerical modelling results. In addition, the pressure variation along the soil–DCM interface was investigated because in practice, DCM walls are designed considering a uniform lateral pressure distribution along the wall length assuming rigid wall movements. The maximum active earth pressure behind the wall was developed at a depth of 11.0 m below the ground surface. Therefore, internal stability of the wall was investigated considering the wall section at 11.0 m depth.

3.3.1 Pressure Distribution at the Soil–DCM Wall Interface

Figure 5 shows the contour plot of normal stress distribution in the direction perpendicular to the face of the excavation developed in soil behind the wall. Figure 6 shows the variation of pressure along the soil–DCM wall interface at a depth of 11 m. The pressure acting on the wide flange is higher than that over the DCM wall section. The pressure along the DCM–soil interface decreases towards the mid-span between two flange beams, and the lowest pressure is recorded at the middle of the span. However, the difference between maximum and minimum pressures is about 10%. The low variation in pressure over the DCM wall section is due to the lower relative movement between steel inclusion and the mid-span of the DCM wall section, when compared to a wall system with soldier piles and timber lagging. For cases with soldier piles and timber lagging, variation of lateral pressure higher than that shown in Fig. 6 was reported in previous studies (MacNab 2002; Perko and Boulden 2008; Vermeer et al. 2001). The relative movement between wide flange columns and DCM wall leads to the formation of soil arching between wide flanges. In practice, the spacing between soldier piles ranges between 1.52 and 3.05 m (Perko and Boulden 2008), which is high compared to the spacing between steel inclusions normally used in DCM walls. The maximum spacing between steel inclusions reported in the literature is 1.7 m (Parmantier et al. 2009), and in this case study the spacing is 1.4 m. Therefore, based on this study, it is reasonable to assume a uniform lateral pressure distribution along the length of DCM walls with steel inclusions.

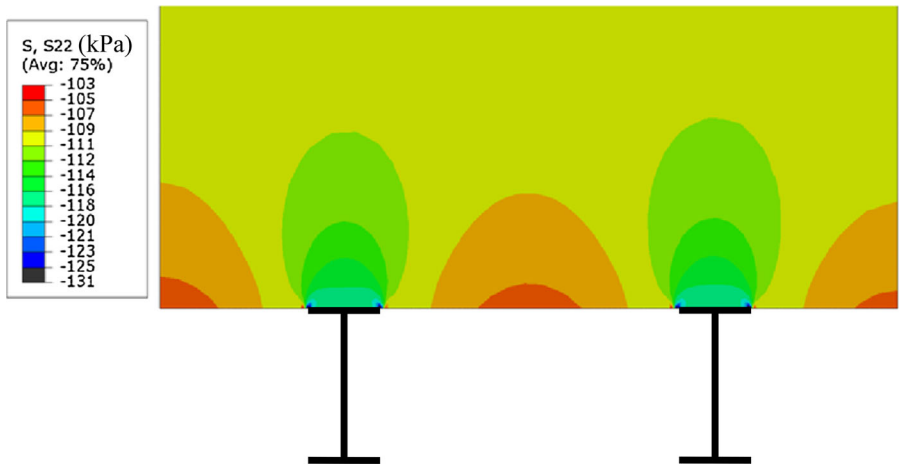

Fig. 5 Contour plot of normal stresses in the excavation direction in soil

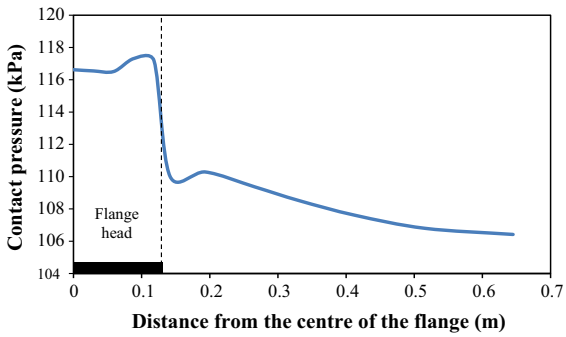

Fig. 6 Variation of Normal contact pressure along the soil–DCM interface

3.3.2 Internal Stability of the Wall with Respect to Bending Failure

Figure 7a, b shows the contour plot of normal stresses developed inside the DCM wall section in kPa. According to the sign convention in ABAQUS, compressive stresses are negative and the tensile stresses are positive. The maximum and minimum stresses are concentrated adjacent to flanges of the steel inclusions, where the end restraints for the arches are formed. A similar stress distribution was observed by Taki and Yang (1991). The compressive strength of DCM wall section is 2 MPa, which is equivalent to the unconfined compressive strength of the cement stabilized soil. The tensile strength of the cement stabilised soil is taken as zero because in practice DCM wall sections are designed to not to take any tensile stresses. According to Fig. 7, the maximum compressive normal stresses developed in the DCM wall section over the horizontal plane in the *X* and *Y* directions (S11 and S22, respectively) are well below the allowable limit of compressive strength. The maximum tensile stresses developed exceed the tensile strength of the wall section. However, according to Fig. 7a, b, the

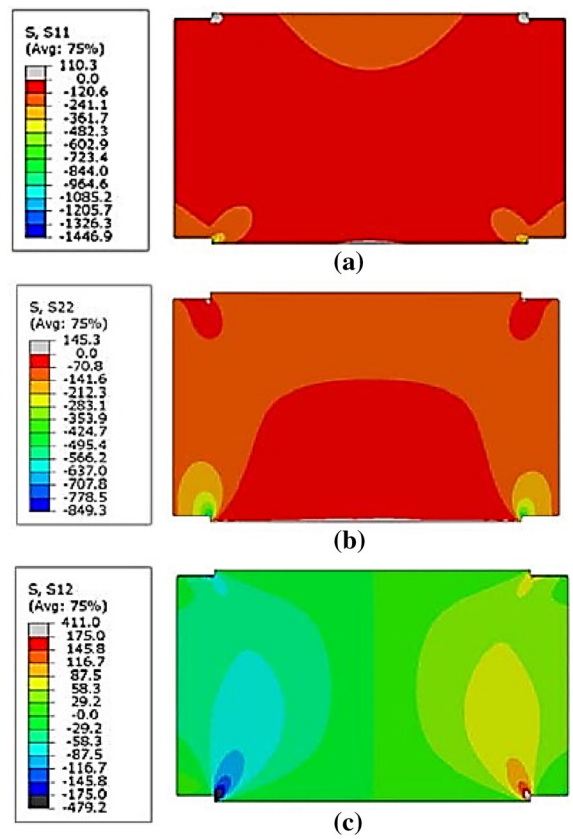

Fig. 7 Contour plots of stresses developed inside DCM block. **a** Normal stress distribution, S11, **b** normal stress distribution, S22, **c** shear stress distribution, S12

grey areas in the contour plots of S11 and S22 near flange tips are extremely small, and hence, it is highly unlikely for those extremely small tensile regions to cause any instabilities in the wall. Therefore, failure of the wall due to bending is highly unlikely.

3.3.3 Internal Stability of the Wall with Respect to Shear Failure

Pearlman and Himick (1993) proposed a method to check the failure against shear based on the American concrete institute guidelines (ACI 318 Code I, 1995), where the nominal shear resistance of the concrete (in units of lbf) is calculated using the following equation:

$$V_c = 2\lambda\sqrt{f_c'} \times b_w \times d_w \tag{1}$$

where λ is 0.75 for light weight concrete, $f_c^{'}$ is the compressive strength of soil cement mix in psi, b_w and d_w are the dimensions of the soil cement block in inches. Equation (1) can be used to calculate the resisting shear force over the cross section of the DCM wall.

According to Ellen et al. (2013), shear strength is calculated using the following equation:

$$v_{\mathrm{DCM}} = \frac{f_r f_{\mathrm{curing}} q_u}{2} \tag{2a}$$

$$f_{\mathrm{curing}} = 0.187 \ln(t) + 0.375 \tag{2b}$$

where f_r is the difference between unconfined peak and confined large-strain strengths, f_{curing} is the curing factor, which can be obtained from Eq. (2b), and q_u is the unconfined compressive strength. f_r ranges from 0.65 to 0.9. Here, a value of 0.65 is used conservatively. Richards and Powrie (1998) proposed the following equation to calculate the shear strength.

$$v_{\mathrm{DCM}} = \frac{q_u}{3} \tag{3}$$

In this analysis, when the 28th day curing strength is considered ($f_{\mathrm{curing}} = 1$ and $q_u = 2000$ kPa), both Eqs. (2a) and (3) yield $v_{\mathrm{DCM}} = 650$ kPa. If the shear stress distribution shown in Fig. 7c is observed, shear stresses, which are concentrated close to the bottom of the flange tips, are about 175 kPa and significantly lower than the shear strength of the DCM wall section. Although the highest shear stress recorded in the contour plot is about 479 kPa, the area over which it is developed is extremely small. Therefore, it can be concluded that the wall is stable against the shear failure.

4 Parametric Study

4.1 Scope of the Study

A parametric study was carried out to investigate the influence of spacing of the wide flange beams, thickness of the DCM wall and the initial lateral earth pressure on the behaviour of DCM walls with steel inclusions. The three-dimensional model presented in the previous section is approximated to a plane strain problem to carry out the parametric study due to the excessive computer time and memory required to carry out three-dimensional finite element modelling for a large number of cases considered in this section. Figure 8 shows the DCM column layout and the steel inclusions used for this analysis. As in practice, the face of the front side of the primary columns was shaved off to facilitate installation of struts for further horizontal support. The horizontal section including two flanges was considered, and the

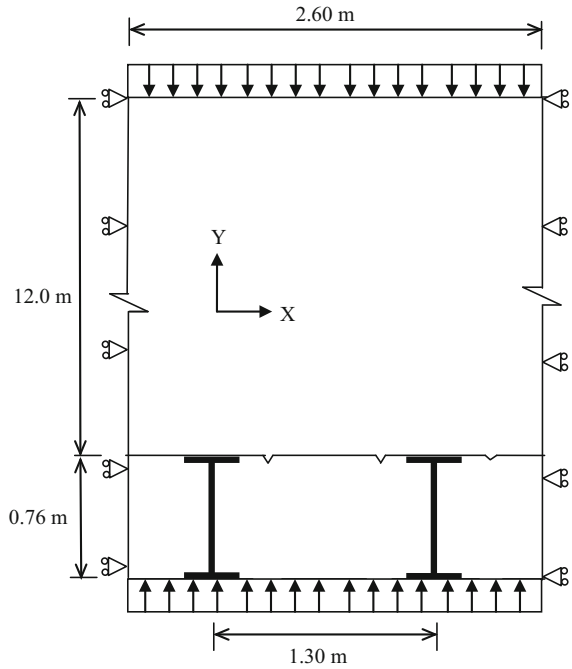

Fig. 8 Geometry of the plane strain model used in the parametric study

soil domain is extended to 12 m behind the wall. In the finite element mesh, the nodes along both sides of the repetitive sections are restrained to move in the X direction and free to move in the Y direction. Initial lateral stress distribution is created by applying a uniform pressure over the front and back faces of the model parallel to the X axis. During the analysis, front face of the flanges is fixed in the first step. To simulate the stress release due to excavation, the pressure applied on the front face of the DCM section is removed.

4.2 Spacing Between Steel Inclusions

Bending failure due to lack of tension capacity of DCM section is highly dependent on the spacing between the wide flange beams. Taki and Yang (1991) proposed a minimum clear distance to be maintained between steel inclusions as shown in Fig. 9 to prevent the bending failure of the wall:

$$L_{cs} < h_f + d_c - 2e \tag{4}$$

where L_{cs} is the clear spacing, h_f is the height of the flange, d_c is the diameter of the DCM column, and e is the distance between the centre of gravity of DCM circular section and wide flange section as shown in Fig. 9. In this analysis, different ratios between spacing, L_{cs}, and the sum of diameter and height of the flange, $h_f + d_c$, are used to check the validity of this criteria.

Table 2 shows the maximum value of normal and shear stresses developed within the DCM section. Compressive strength of the DCM section used for this analysis was 2 MPa. In practice, tensile strength of the cement stabilized soil is taken as 10% of the compressive strength (Briaud et al. 2000). In this study, a tensile strength of zero is assumed for the DCM section, because normally practicing engineers

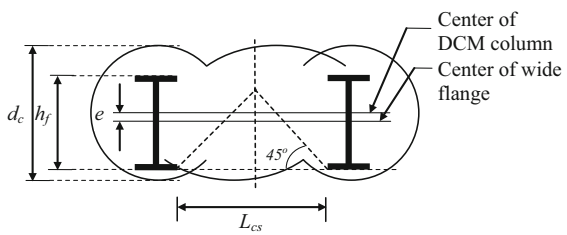

Fig. 9 Cross section of DCM wall with steel inclusions (after Taki and Yang 1991)

carry out design of DCM columns assuming zero tensile strength for columns. That means when the stresses are below zero, the region is defined as a failed zone. Maximum allowable shear strength is computed according to Eq. (1), and the shear strength is equal to 650 kPa.

If we consider these limits for stresses, none of the cases considered above are viable against bending failure. However, the maximum stresses are found to be developed over a very small area. Hence, the maximum or minimum stresses developed alone cannot be used as a guide to check the viability of the section. Hence in this study, the area over which the stresses exceeded the limiting stresses is computed as a percentage of the area of the DCM section between the wide flange steel inclusions. The compressive stresses exceeded the limiting values over an area less than 0.01% of the total DCM wall section between flanges. Therefore, we can conclude that the compressive stresses due to bending are not critical and will not cause failure of the composite wall system. In what follows, only tensile stresses and shear stresses developed within the wall section are considered to determine the internal stability of the wall.

Figure 10a shows the failed area where tensile stresses are greater than zero and shear stresses are greater than the shear strength, as a percentage of DCM wall area between flanges. The length of the cracked region shown in Y axis of Fig. 10b is calculated using the length of the tension zone at the critical section (middle of the span) and the length of the region over which shear stresses exceed the shear strength (near the tip of the flange) as a percentage of the thickness of the DCM wall. The area and the length of the failed region increase with the increasing spacing between flange beams as expected due to higher loading applied over the wall section between steel inclusions. Tension (S11) developed due to the sagging of DCM region between steel inclusions causes substantial amount of failed area. The failure zone increases considerably with increasing spacing between steel inclusions. Even though the magnitude of tension developed in the direction of soil movement (S22) given in Table 2 is higher than that developed due to S11, the area and the length of the failed region due to S22 are very small. For all cases with $L_{cs}/(h_f + d_c) < 1.0$, the shear stresses are within the limits according to the Mohr–Coulomb yield criteria and the proposed failure criteria based on Eqs. (2a) and (3).

Table 2 Maximum value of stresses developed within the DCM section for different spacing of steel inclusion

$L_{cs}/(h_f + d_c)$	0.6	0.8	1	1.2	1.5
Spacing between inclusions (m)	1.3	1.6	1.934	2.27	2.77
Max tension, S11 (kPa)	6	34.5	84	132	220
Max tension, S22 (kPa)	150	178	226	260	323
Max compression, S11 (kPa)	1474	1880	2453	2870	3705
Max compression, S22 (kPa)	850	930	1121	1220	1430
Max shear, S12 (kPa)	481	587	747	860	1090
Max mid-span deflection (mm)	0.6	0.7	1.2	1.8	3

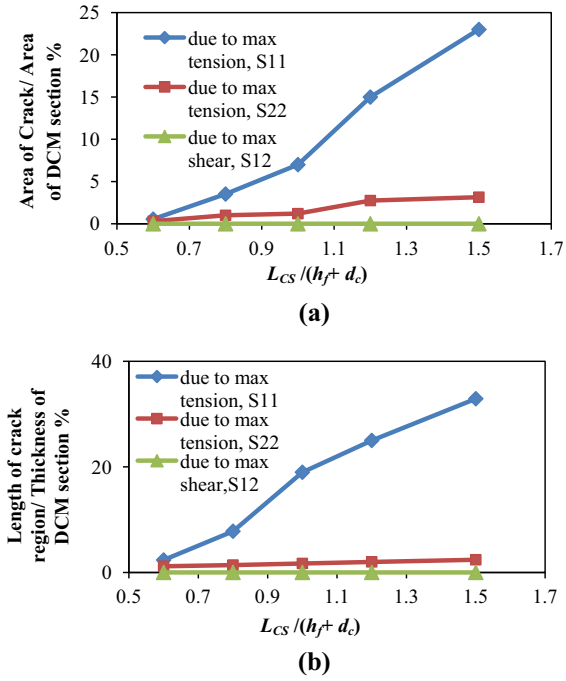

Fig. 10 Influence of spacing of steel inclusions on the failure zone. **a** Failure zone defined using area of crack, **b** failure zone defined using length of crack

When $L_{cs}/(h_f + d_c) > 1.0$, developed shear stresses exceeded the limits over a very small region as shown in Fig. 10.

If Eq. (4) is rearranged with $L_{cs}/(h_f + d_c)$, which is the critical spacing ratio, as shown in Eq. (5) below, it is clear that when e increases, the critical spacing ratio decreases below 1 to avoid bending failure. Therefore, to achieve an economical arrangement of steel inclusions, e should be zero. That means the centre of the flange beams and DCM wall section should coincide.

$$\frac{L_{cs}}{(h_f + d_c)} < 1 - \frac{2e}{(h_f + d_c)} \tag{5}$$

Results presented in this section were obtained with zero e as shown in Fig. 8. However, according to Fig. 10, to avoid any tension cracks, the critical spacing ratio should be a value less than what is given by Eq. (5), when e is zero. Therefore, a new equation can be proposed to avoid the development of any tension cracks as shown below:

$$\frac{L_{cs}}{(h_f + d_c)} \leq 0.6 \tag{6}$$

4.3 Thickness of the DCM Layer

Over recent years, Cutter Soil Mixing (CSM) technique is widely used instead of conventional DCM method to construct cement stabilised walls. In the CSM technique, rectangular overlapping panels are created using two counter rotating wheels in the vertical plane. Hence in this section instead of diameter of DCM columns, different thicknesses of DCM sections are considered as a multiple of h_f, because h_f and d_c are the key parameters in determining the spacing between wide flanges (Taki and Yang 1991).

Table 3 shows the maximum values of stresses developed within the DCM section for different thicknesses of DCM wall. Figure 11a, b shows the variation of area and length of the failure zone as a percentage of the area of DCM section and the flange height (h_f) with thickness of the DCM section. The increase in thickness helps to reduce the extent of tensile stresses developed in the transverse direction significantly. Based on the results presented in Fig. 11, the critical thickness ratio, d_c/h_f, to avoid any tension cracks in the DCM wall section is given by,

$$\frac{d_c}{h_f} \geq 2 \tag{7}$$

Table 3 Maximum value of stresses developed within the DCM section for different thickness of DCM wall

Thickness of the DCM layer	h	1.25 h	1.5 h	1.75 h	2 h
Max tension, S11 (kPa)	84	70	50	9	4
Max tension, S22 (kPa)	226	212	193	175	171
Max compression, S11 (kPa)	2453	2290	2110	1840	1799
Max compression, S22 (kPa)	1121	1057	935	913	898
Max shear, S12 (kPa)	747	702	650	573	564
Max mid-span deflection (mm)	1.2	1	1	0.8	0.7

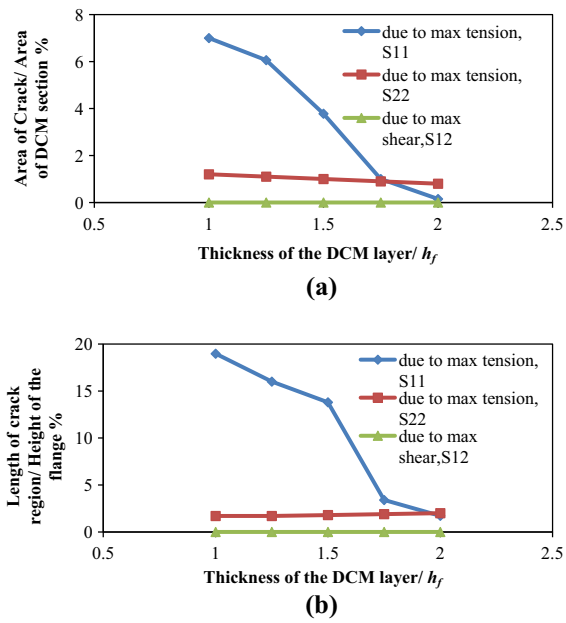

Fig. 11 Influence of thickness of DCM wall on the failure zone. **a** Failure zone defined using area of crack, **b** failure zone defined using length of crack

However, the increase in DCM wall thickness does not have a significant influence on the extent of the tensile stresses developed in the direction of the soil movement (Direction *Y* in Fig. 5). For all cases shear stresses are within the limits.

By rearranging Eq. (6), the distance between steel inclusions can be given by the following equation:

$$\frac{L_{cs}}{h_f} \leq 0.6\left(1+\frac{d_c}{h_f}\right) \tag{8}$$

Based on Eqs. (7) and (8), distance between steel inclusions, L_{cs}, DCM wall thickness, d_c, and flange beam height, h_f, can be determined to avoid the development of any tensile cracks in the DCM wall section.

4.4 Different Initial Lateral Earth Pressures

Different initial lateral earth pressures, which represent different depths of excavation, were considered to check the viability of the DCM section with steel inclusions. Figure 12 shows the variation of contact pressures along the DCM–soil interface. The pressure distribution does not depend on the initial lateral earth pressures. The contact pressure over the flange is 6% higher than the initial lateral earth pressure, while the contact pressure over the mid-span of the DCM–soil interface is 4% less than the applied initial lateral earth pressure. Here, a small variation of contact pressure is observed due to the small relative movement between DCM section and the flange.

Table 4 shows the variation of stresses and the mid-span deflection with respect to the deflection of wide flange beams with the increasing initial pressures. Figure 13a, b shows the area and the length of the failed zone for different initial lateral earth pressures as a percentage of area and length of the DCM section used.

Even though the maximum stresses developed increase with increasing initial lateral earth pressure, the area or length of failed zone is very small when compared to the cases considered in the previous

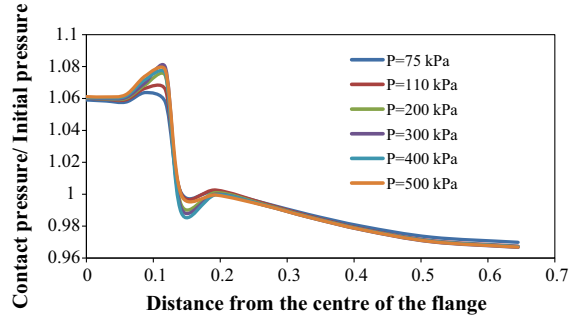

Fig. 12 Variation of normal contact pressure along the soil–DCM interface for different lateral earth pressures

Table 4 Maximum value of stresses developed within the DCM section for different lateral earth pressures

Initial pressure (kPa)	P = 75	P = 110	P = 200	P = 300	P = 400	P = 500
Max tension, S11 (kPa)	2.5	6	12	18	28	38
Max tension, S22 (kPa)	102	150	263	420	569	647
Max compression, S11 (kPa)	1000	1474	2668	3898	4464	4662
Max compression, S22 (kPa)	578	850	1554	2375	3242	3912
Max shear, S12 (kPa)	327	481	887	1425	1862	2084
Max mid-span deflection (mm)	0.4	0.6	1	1.6	2.1	2.6

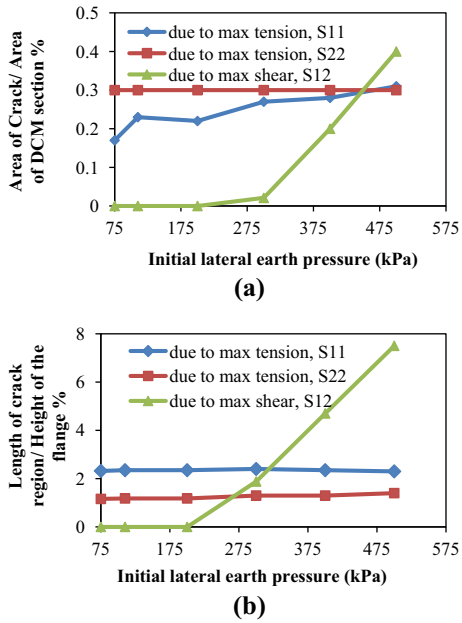

Fig. 13 Influence of initial lateral earth pressure on failure zone. **a** Failure zone defined using area of crack, **b** failure zone defined using length of crack

section as shown in Fig. 13. Deeper excavations cause larger failure zone due to high shear stresses developed in the wall in excess of shear strength. However, it does not have much impact on the variation of failure zone caused by tensile stresses (S11 and S22). When the initial lateral pressure is very high (P = 500 kPa), only small amount of yielding was observed in the DCM section near the tip of the flanges.

5 Conclusion

This paper investigated the performance of earth retaining structures constructed using DCM columns with steel inclusions. An extended version of the Mohr–Coulomb model has been used to represent the constitute behaviour of DCM columns incorporating the strain-softening behaviour of cement stabilised soils beyond yield. A case study was modelled using a three-dimensional finite element model. Predicted deformation using the finite element analysis agrees well with the measured data. The internal stability of the DCM wall section was investigated against bending and shear failure modes of the wall because other three rigid body motions for rotation, lateral deformation and settlement are not significant for this wall. Shear and normal stress distributions show that they are within the allowable limits, and hence, there is no likelihood for failure of the wall. Due to the relative movement between flanges and the DCM section, there is a pressure variation over the wall section and leads to the formation of soil arching between flange beams. However, the pressure variation over the wall length is less than 10% and it is reasonable to assume a uniform pressure distribution for planar DCM walls with steel inclusions.

A detailed parametric study was carried out investigating the influence of spacing between flanges, thickness of the DCM wall and the excavation depth on the behaviour of the DCM wall with steel inclusions. Results of the parametric study show that it is difficult to discuss the failure of the section by considering only the maximum stresses. In some cases, although stresses exceeded the allowable limits, area over which they exceeded was very small. Hence, parametric study results were evaluated considering two criteria: (i) cracked area as a fraction of the area of the DCM section and (ii) length of cracked region as a fraction of the thickness of the DCM section. With the increase in distance between wide flanges and decrease in thickness of the DCM wall, tensile stresses developed due to bending of the wall between flanges in the horizontal plane significantly increase. Based on these results, two equations are proposed to select the

wall thickness and spacing between steel inclusions based on the height of the steel flange beam.

The initial lateral pressure applied over the wall section was changed to simulate the wall behaviour for different excavation depths. Results show that the normal contact pressure variation along the DCM–soil interface was not significantly different to the applied lateral earth pressure due to the little relative movement between DCM and flange sections of the wall cross section. With the increase in lateral earth pressure, size of the failure zone due to tensile stresses has not been changed significantly, but the likelihood for failure due to shear increases at larger lateral earth pressures (or excavation depths).

Acknowledgements The authors would like to acknowledge the financial assistance provided by the Australian Research Council for this research under the Discovery Grant DP1094309.

References

American Concrete Institute Committee (1995) Building code requirements for reinforced concrete (ACI 318-01). American Concrete Institute, Farmington Hills

Arroyo M, Ciantia M, Castellanza R, Gens A, Nova R (2012) Simulation of cement-improved clay structures with a bonded elasto-plastic model: a practical approach. Comput Geotech 45:140–150

Blackwell J (1992) A case history of soil stabilization using the mix-in-place technique for the construction of deep manhole shafts at Rochdale. In: Grouting in the Ground. London, pp 497–509

Briaud JL, Nicholson P, Lee J (2000) Behavior of a full-scale VERT wall in sand. J Geotech Geoenviron Eng 126(9):808–818

Broms BB (1999) Design of lime, lime/cement and cement columns. In: Dry mix methods for deep soil stabilisation, pp 125–154

Capelo A, Correia AG, Ramos LF, Pinto A, Tomasio R (2012) Modelling and monitoring of an excavation support using CSM. In: Proceedings of the 4th international conference on grouting and deep mixing 2012, Geotechnical special publication 228, New Orleans, Louisiana, February 15–18, pp 243–250

Ellen M, Bruce C, Berg RR, Collin JG, Filz GM, Terashi M, Yang DS (2013) Federal Highway Administration design manual: deep mixing for embankments and excavation support. Federal Highway Administration, Washington, DC

EuroSoilStab (2002) Development of design and construction methods to stabilize soft organic soils: design guide soft soil stabilization. CT97-0351, Project No: BE 96-3177

Gerressen FW, Vohs T (2012) CSM-cutter soil mixing—worldwide experiences of a young soil mixing method. In: Grouting and deep mixing 2012, Geotechnical special publication 228, New Orleans, Louisiana, February 15–18, pp 282–290

Huang J, Han J, Oztoprak S (2009) Coupled mechanical and hydraulic modelling of geosynthetic-reinforced column-supported embankments. J Geotech Geoenviron Eng 135(8):1011–1021

Lai YP, Bergado DT, Lorenzo GA, Duangchan T (2006) Full-scale reinforced embankment on deep jet mixing improved ground. Ground Improv 10(4):153–164

Lee K, Chan D, Lam K (2004) Constitutive model for cement treated clay in a critical state framework. Soils Found 44(3):69–77

Lopez RA, Majewski A, Harvey T (2009) Permanent excavation support in urban areas using cutter soil mixing technology: Elliott Avenue case history, Seattle, Washington, Geo-Florida 2009. In: Contemporary topics in ground modification, problem soils, and geo-support, Geotechnical special publication 187, pp 185–192

MacNab A (2002) Earth retention systems handbook. McGraw-Hill, New York, pp 319–322

McGinn AJ, O'Rourke TD (2003) Performance of deep mixing methods at Fort Point Channel. Federal Highway Administration, Washington, DC

Nguyen L, Fatahi B (2016) Behaviour of clay treated with cement & fibre while capturing cementation degradation and fibre failure—C3F Model. Int J Plast 81:168–195

Nguyen L, Fatahi B, Khabbaz H (2014) A constitutive model for cemented clays capturing cementation degradation. Int J Plast 56:1–18

Nicholson PJ, Mitchell JK, Bahner EW, Moriwaki Y (1998) Design of a soil mixed composite gravity wall. In: Soil improvement for Big Digs, Geotechnical special publication 81, Geo-Congress 98 October 18–21, Boston, Massachusetts, USA, pp 27–40

Okumura T (1996) Deep mixing method of Japan. In: Grouting and deep mixing, proceedings of the second international conference on ground improvement geosystems, Tokyo, Japan, 14–17 May, pp 879–887

Ou CY, Wu TS, Hsieh H (1996) Analysis of deep excavation with column type of ground improvement in soft clay. J Geotech Eng 122(9):709–716

Parmantier DM, Stow RFP, Byrne RJ (2009) Case study: cement–bentonite pre-trenching and cutter soil mixing (CSM) for temporary shoring and ground water cut-off. In: Contemporary topics in ground modification, problem soils and geo-support, proceedings of the international foundation Congress and equipment expo, held in Orlando, Florida, USA, March 15–19, 2009 pp 153–160

Pearlman SL, Himick DE (1993) Anchored excavation support using SMW. In: Deep Foundation Institute, 18th annual conference, Pittsburgh, PA, USA, pp 101–120

Perko HA, Boulden J (2008) Lateral earth pressures on wood lagging in soldier pile earth shoring systems. J Deep Found Inst 2:52–60

Porbaha A, Shibuya S, Kishida T (2000) State of the art in deep mixing technology: part III. Geotechnical characterization. Ground Improv 3:91–110

Potts DM, Dounias GT, Vaughan PR (1990) Finite-element analysis of progressive failure of Carsington embankment. Geotechnique 40(1):79–101

Potts DM, Kovacevic N, Vaughan PR (1997) Delayed collapse of cut slopes in stiff clay. Geotechnique 47(5):953–982

Quiroga AJ, Thompson ZM, Muraleetharan KK, Miller GA, Cerato AB (2017) Stress–strain behaviour of cement-improved clays: testing and modelling. Acta Geotech 12:1003–1020

Richards DJ, Powrie W (1998) Centrifuge model tests on doubly propped embedded retaining walls in overconsolidated Kaolin clay. Geotechnique 48:833–846

Rutherford CJ, Biscontin G, Briaud JL (2005) Deformation predictions based on estimates of soil cement modulus and flexural stiffness. In: Proceedings, the 11th international conference of IACMAG, June 19–24, 2005, Turin, Italy, vol 3, pp 433–440

Rutherford CJ, Biscontin G, Koutsoftas D, Briaud JL (2007) Design process of deep soil mixed walls for excavation support. Int J Geoeng Case Hist 1(2):56–72

Shao Y, Zhang C, Macari EJ (1998) The application of deep mixing pile walls for retaining structures in excavations. In: Soil Improvement for Big Digs, Geotechnical special publication 81, Geo-Congress 98 October 18–21, Boston, Massachusetts, USA, pp. 84–95

Shao Y, Macari EJ, Cai W (2005) Compound deep soil mixing columns for retaining structures in excavations. J Geotech Geoenviron Eng 131(11):1370–1377

Stoetzer E, Brunner WG, Fiorotto R, Gerressen FW, Schoepf M (2006) Cutter soil mixing—a new technique for the construction of subterranean walls initial experiences gained on completed projects. In: Proceedings of DFI/EFFC 10th international conference on piling and deep foundations, Amsterdam, The Netherlands, Publication no. 77

Suebsuk J, Horpibulsuk S, Liu MD (2010) Modified structured cam clay: a generalised critical state model for destructured, naturally structured and artificially structured clays. Comput Geotech 37(7–8):956–968

Taki O, Yang DS (1991) Soil–cement mixed wall technique. In: ASCE special conference, Denver, CO, USA, pp 298–309

Vatsala A, Nova R, Sirinivasa Murthy BR (2001) Elastoplastic model for cemented soils. J Geotech Geoenviron Eng 127(8):678–687

Vermeer PA, Punlor A, Ruse N (2001) Arching effects behind a soldier pile wall. Comput Geotech 28(6–7):379–396

Yang DS (2003) Soil–cement walls for excavation support. In: Earth retention systems: 2003, A Joint Conference presented by ASCE Metropolitan Section of Geotechnical Group, The Deep Foundations Institute, and The International Association of Foundation Drilling, New York, USA, pp 1–17

Yapage NNS, Liyanapathirana DS, Poulos HG, Kelly RB, Leo CJ (2015) Numerical modeling of geotextile-reinforced embankments over deep cement mixed columns incorporating strain-softening behavior of columns. Int J Geomech 15(2):04014047